

## **Bondbreaking without barriers. II. Vibrationally excited products**

William H. Green Jr., Arthur J. Mahoney, QiKe Zheng, and C. Bradley Moore

Citation: *The Journal of Chemical Physics* **94**, 1961 (1991); doi: 10.1063/1.459918

View online: <http://dx.doi.org/10.1063/1.459918>

View Table of Contents: <http://scitation.aip.org/content/aip/journal/jcp/94/3?ver=pdfcov>

Published by the [AIP Publishing](#)

---

### **Advertisement:**



## Re-register for Table of Content Alerts

Create a profile.



Sign up today!



# Bond-breaking without barriers. II. Vibrationally excited products

William H. Green, Jr.,<sup>a)</sup> Arthur J. Mahoney, Qi-Ke Zheng,<sup>b)</sup> and C. Bradley Moore  
*Department of Chemistry, University of California, Berkeley, Berkeley, California 94720*

(Received 23 April 1990; accepted 16 October 1990)

Ketene is photolyzed in a supersonic jet, and the vibrationally excited singlet methylene  $\text{CH}_2$  ( $\tilde{a}^1A_1$ ), produced is detected by laser-induced fluorescence. The appearance thresholds and yield curves of individual methylene rovibrational states are obtained by scanning the photolysis laser wavelength. As observed previously by probing the (0,0,0) state at lower photolysis energies, there are no barriers to dissociation and nuclear spin is conserved. Sharp steps are observed just above the energetic threshold in each of these photofragment excitation (PHOFEX) curves. This suggests that the rotational state distributions are given by phase space theory (PST). The quantum yield of the (0,1,0) $1_{01}$  rovibrational state is measured and the quantum yield for (0,1,0) inferred. These values are larger than predicted by PST, and are close to values predicted by variational Rice–Ramsberger–Kassel–Marcus (RRKM) theory and by the separate statistical ensembles (SSE) method. This indicates that near the (0,1,0) energy threshold the (0,0,0) yield is constrained, as by a tight transition state. The appearance of steps spaced by the energies of a free CO rotor in the PHOFEX curves close to the thresholds of each vibrational state probed indicates that the near threshold flux of vibrationally excited products is controlled by a loose “transition state” on a vibrationally adiabatic surface. These observations are consistent with the variational RRKM theory for dissociations without barriers in which each product vibrational state evolves on its own vibrationally adiabatic potential surface and has its own transition state. As the energy increases above the threshold for a vibrational state, its transition state moves in along the reaction coordinate and tightens. Thus total rates increase less rapidly with energy than in PST and vibrational distributions are skewed towards higher levels than in PST.

## I. INTRODUCTION

Historically, theories for unimolecular reactions have been developed for and tested against thermal reaction rate measurements.<sup>1–7</sup> For bond breaking on potential energy surfaces without a barrier to fragment recombination there is no obvious way to locate the position of a transition state along the reaction coordinate. The phase space theory (PST)<sup>3,4</sup> provides an asymptotic limit by locating the transition state at infinity (separated fragments). The Rice–Ramsberger–Kassel–Marcus (RRKM) theory<sup>1,2</sup> and the statistical adiabatic channel model (SACM)<sup>5–7</sup> provide alternative models. Recent advances in laser and molecular beam technology permit much finer control of the energetics and much better temporal resolution. Measurements of rate constants,<sup>8,9</sup> product energy distributions<sup>10–14</sup> and photofragment excitation spectra<sup>15–17</sup> near product energy state thresholds have provided particularly sensitive probes of reaction dynamics. New theories such as variational RRKM<sup>18–20</sup> and separate statistical ensembles (SSE)<sup>10,21</sup> have been developed.<sup>22</sup> The production of vibrationally excited fragments provides a particularly sensitive test of alternative models for transition state location.<sup>5,19,22</sup>

The lowest electronic states of ketene illustrated in Fig. 1 reflect the results of recent *ab initio* calculations and spectroscopic and dynamic measurements.<sup>15,23–28</sup> After excita-

tion to the  $S_1$  state, the molecule undergoes rapid internal conversion and/or intersystem crossing to the lower electronic states, followed by dissociation. The absorption spectrum of ketene is diffuse and no fluorescence has been observed. The singlet channel dissociation dominates from a few hundred  $\text{cm}^{-1}$  above its reaction threshold; the branching ratio with the triplet channel is reported in the preceding paper.<sup>14</sup> One advantage of the ketene system for testing theories of unimolecular dissociation is that the ketene absorption spectrum is not structured; this allows smooth variation in the total energy available while the dissociation rate or the yield of a particular product state is probed. The PHOFEX technique is especially useful near the appearance thresholds of the various states, where the PHOFEX spectra exhibit structure which is sensitive to the properties of the transition state which determines the product vibrational state distribution.

## II. EXPERIMENTAL

Ketene is seeded in helium carrier gas and cooled by supersonic expansion into a vacuum chamber. The cold ketene is photolyzed with a pulse of tunable uv light (303–332 nm), and the singlet methylene produced is excited with a visible pulse (560–640 nm). The methylene fluorescence is detected with a red-sensitive photomultiplier tube (PMT) through appropriate filters. To measure PHOFEX spectra the uv wavelength is scanned, while for the branching ratio measurement the visible wavelength is scanned.

The apparatus and techniques are nearly identical to those used in the previous PHOFEX study,<sup>15–17</sup> so only

<sup>a)</sup> Present address: University Chemical Laboratory, Lensfield Rd., Cambridge CB2 1EW, England.

<sup>b)</sup> Present address: Department of Physics II, Fudan University, Shanghai, People's Republic of China.

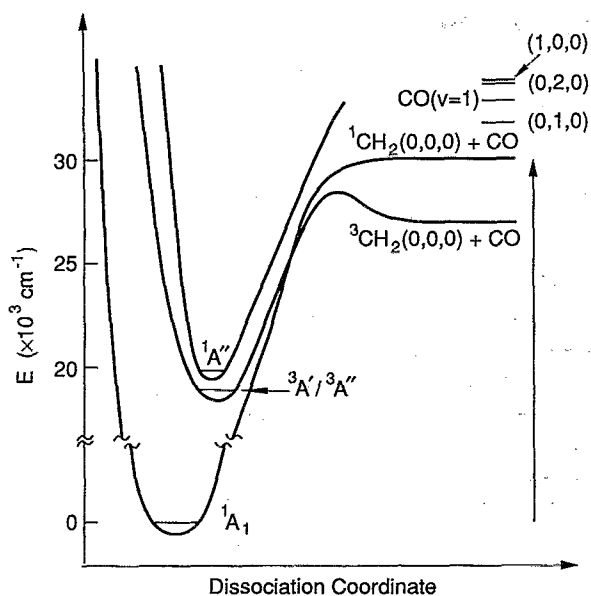


FIG. 1. The potential energy surfaces of the low-lying electronic states of ketene. Indicated are the singlet threshold energy,  $30\,116.2\text{ cm}^{-1}$ ; and the energies relative to the singlet threshold of the  $(0,1,0)$  channel,  $1352.5\text{ cm}^{-1}$ ;  $\text{CO}(v=1)$ ,  $2143.2\text{ cm}^{-1}$ ; the  $(0,2,0)$  channel,  $2667.7\text{ cm}^{-1}$ ; and the  $(1,0,0)$  channel,  $2806.0\text{ cm}^{-1}$ .

changes are noted here. The U tube containing the liquid ketene has been replaced with a bubbler, and kept filled with a larger amount of ketene, so that He bubbles flow through several cm of ketene before entering the pulsed valve. This improves the stability of the partial pressure of ketene vapor picked up by the carrier gas. The vacuum line has also been modified so that it can handle higher backing pressures. Most of the results presented here were measured using 2 atm backing pressure of He seeded with  $\approx 50$  Torr of ketene (hexanes slush); under these conditions, the ketene temperature in the beam is expected to be less than  $4\text{ K}$ .<sup>15,16</sup>

The photolysis laser system used in the previous study was replaced by a more powerful Quantel YG-580 Nd:YAG pumping a Quantel TDL-50 dye laser, with a nominal resolution of  $0.1\text{ cm}^{-1}$ . The dye laser wavelength was controlled by a Fountain PC microcomputer, through a Metrabyte DASH-8 interface, with software developed in this laboratory. After frequency doubling by KDP in an InRad Auto-tracker II, this system produced 5–12 mJ of ultraviolet light. The second harmonic was separated from the fundamental by four reflections from dichroic mirrors. As in the previous study, the signal was normalized to the UV power coming through the beam machine using a Moletron J-9 pyroelectric detector.

The fluorescence collection has been significantly improved by moving the photomultiplier closer to the interaction region and adding a 7 cm diameter, 5 cm front f.l. aspheric glass lens between the interaction region and the PMT, and a 6 cm diameter, 5 cm radius of curvature spherical aluminum mirror opposite the interaction region. The lens acts as a field lens for the mirror, as well as a collimating lens in its own right; together the two improve the collection efficiency by at least a factor of 2.

Because the singlet methylene LIF spectrum is highly congested when methylene is formed with sufficient energy to access vibrationally excited states, it is necessary to separate the fluorescence due to the vibrationally excited states from the large background originating from  $v''=0$  rotational states. This is accomplished by using short-pass filters which only pass fluorescence blueshifted from the excitation wavelength. In the present experiment, transitions to the region of the  $\tilde{b}(0,15,0)$  vibrational band are used exclusively; when detecting vibrationally excited methylene, two Ealing 580 nm short-pass interference filters (preceded by Schott glass BG14 when needed) allow only fluorescence to the  $\tilde{a}(0,0,0)$  state to be detected. When measuring transitions from  $(0,0,0)$ , no blueshifted fluorescence is expected, and red Schott glass RG630 is used instead to block the scattered laser light.

The improved photolysis power and collection efficiency, coupled with the ability to separate LIF transitions originating from different vibrational states, allowed detection and unambiguous assignment of previously unknown singlet methylene rovibronic transitions originating from  $\tilde{a}(0,1,0)$ ,  $(0,2,0)$ , and  $(1,0,0)$ . These spectroscopic results are reported separately.<sup>27,29</sup> PHOFEX spectra measured using some of these new transitions are reported in the present work.

In deconvoluting the data, it is necessary to know the absorption spectrum of ketene. The room temperature measurement<sup>30</sup> has been repeated using a Hewlett-Packard 8450 uv/vis spectrometer in order to obtain a more detailed spectrum. A low temperature, or, preferably, jet-cooled spectrum would be best for the present purposes, but none is available.

The branching ratio between  $(0,1,0)$  and  $(0,0,0)$  was measured by saturating LIF transitions to the same upper state. This was necessary because absolute line strength factors are not known for the singlet methylene transitions, and the signal:noise ratio is best for large probe laser powers. The transitions employed are  $\tilde{b}(0,15,0)2_{11} \leftarrow \tilde{a}(0,1,0)1_{01}$  at  $16\,405.28\text{ cm}^{-1}$  and  $\tilde{b}(0,15,0)2_{11} \leftarrow \tilde{a}(0,0,0)1_{01}$  at  $17\,757.76\text{ cm}^{-1}$ . To confirm that the transitions can be saturated, the LIF intensity was measured as a function of laser power. Though the measured intensity does increase slightly with power, the signal becomes nearly independent of laser power once power broadening becomes evident in the LIF spectra. For the branching ratio measurement, the probe laser power was adjusted so that the FWHM linewidth of the desired transition was  $0.5\text{ cm}^{-1}$  (with a laser linewidth of  $0.2\text{ cm}^{-1}$  and a Doppler width of less than  $0.1\text{ cm}^{-1}$ ). Under these conditions, the transitions should be equally saturated, and the ratio of the peak fluorescence intensities of the two transitions should equal the ratio of the lower state populations.

There are further complications in making this measurement. Due to the congestion in the methylene spectrum, it is not possible at  $0.5\text{ cm}^{-1}$  resolution to avoid overlaps in the  $(0,0,0)$  LIF spectrum at the short photolysis wavelengths needed to produce  $(0,1,0)$ . Also, the rotational state distribution of  $(0,0,0)$  is not known at such high energy; it is certainly possible that it is not given by PST theory as it is at

lower energy. To avoid these problems, the yield of  $(0,0,0)1_{01}$  was measured at a longer photolysis wavelength, where the spectrum is not congested, and where the previous work<sup>15,16</sup> has established that the rotational state distribution is indeed given by PST theory. This approach has the disadvantage that the triplet channel is more important at low energy; however, the behavior of the triplet channel is understood, and can be corrected for using data from the preceding paper.<sup>14</sup> The factors needed to convert the experimental peak heights to the  $(0,1,0)$  quantum yield are discussed in detail in Sec. VI A.

One last complication is that different filters must be used for probing the different transitions. To remove the scattered laser light and measure the  $(0,0,0)$  LIF spectrum, red long-pass filters must be used. But to remove overlapping  $(0,0,0)$  transitions from the  $(0,1,0)$  LIF spectrum—serious interferences at high laser powers where all the transitions are power broadened—it is necessary to use the blue short-pass filters. The relative sensitivity, which depends on the Franck–Condon factors of the fluorescence and the wavelength-dependent efficiency of the PMT, was measured by repeatedly exchanging the two filter stacks while exciting the  $\bar{b}(0,15,0)2_{11} \leftarrow \bar{a}(0,1,0)1_{01}$  transition with low probe laser power and the pump laser at  $31\,564.8\text{ cm}^{-1}$ . The blue detection system was found to be more sensitive to the  $\bar{b}(0,15,0)2_{11}$  fluorescence than the red system by a factor of  $2.8 \pm 0.3$ . The accuracy of this measurement is limited by overlaps with the wings of two nearby unassigned  $(0,0,0)$  peaks, see Fig. 2.

The actual branching ratio measurement was carried out by changing the photolysis and probe dye laser wavelengths while maintaining a fixed laser alignment. It was possible, using fixed irises as guides, and after some practice, to reproducibly readjust both laser beams to the optimal alignment through the interaction region after the optics had been randomly misaligned. This was fortunate, as it proved convenient to change the probe laser dye by changing the dye cuvettes and circulators in order to obtain the new probe wavelength; this certainly misaligned the probe laser beam. Then the LIF spectrum in the region of the transition of interest was scanned, the probe power adjusted to make the linewidth  $0.5\text{ cm}^{-1}$ , and the spectrum scanned again. The

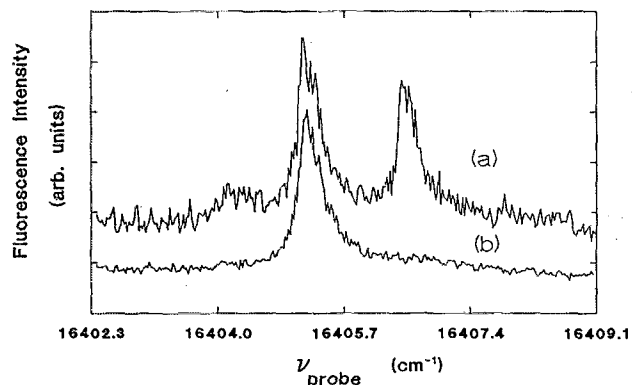


FIG. 2. LIF spectra in the  $\bar{b}(0,15,0)2_{11} \leftarrow \bar{a}(0,1,0)1_{01}$  transition region as viewed through (a) the red filters and (b) the blue filters.

whole procedure was repeated several times to ensure reproducibility.

Reproducibility of the photolysis frequency could potentially be a serious source of error in measuring this ratio, as the PHOFEX curves of the states probed are highly structured. To allow reproducible changes in the photolysis laser wavelength, at each iteration the photolysis laser fundamental was tuned on to either the Ne optogalvanic line at  $633.618\text{ nm}$  or the one at  $660.078\text{ nm}$ . The corresponding photolysis frequencies are  $31\,564.8\text{ cm}^{-1}$  for the  $(0,1,0)$  measurement (Fig. 5) and  $30\,299.4\text{ cm}^{-1}$  for the  $(0,0,0)$  measurement, a few  $\text{cm}^{-1}$  above the  $\text{CO}(J=9)$  threshold, see Fig. 2 of Ref. 15. Precise wavelength reproducibility is not an issue for the probe laser, since it was scanned over the peak to obtain the LIF spectrum.

### III. PHOFEX SPECTRA

#### A. Results

The PHOFEX spectrum for  $(0,1,0)1_{01}$ , Fig. 3, is qualitatively similar to the PHOFEX spectra of  $\bar{a}(0,0,0)$  rotational states reported previously.<sup>15,16</sup> At these energies at least two-thirds of the reactive flux yields  $\bar{a}(0,0,0)$  product.<sup>14</sup> As for  $(0,0,0)$ , the steps in this spectrum are spaced by the rotational term values of the CO product indicating that the quantum yield of this rovibronic state is determined at a large enough value of the reaction coordinate that the energy eigenvalues are essentially those of the isolated fragment molecule. The threshold, measured precisely using the sharp steps as in the previous work,<sup>15,16</sup> lies at  $31\,477.0 \pm 0.5\text{ cm}^{-1}$ —compared to the energetic threshold of  $31\,477.2 \pm 0.4\text{ cm}^{-1}$  expected<sup>15,25</sup> if there is no barrier and if nuclear spin is conserved. Figure 4 shows PHOFEX spectra for a variety of  $(0,1,0)$  states and Table I lists the thresholds for these  $(0,1,0)$  states determined by fitting the experimental curves near the threshold to simulated spectra as was done in previous work.<sup>15,16</sup> As was the case with  $(0,0,0)$  states, there are no detectable barriers for the  $(0,1,0)$  states; the deviation from the energetic threshold is within the uncertainty of the measurement. The absence of any barrier for

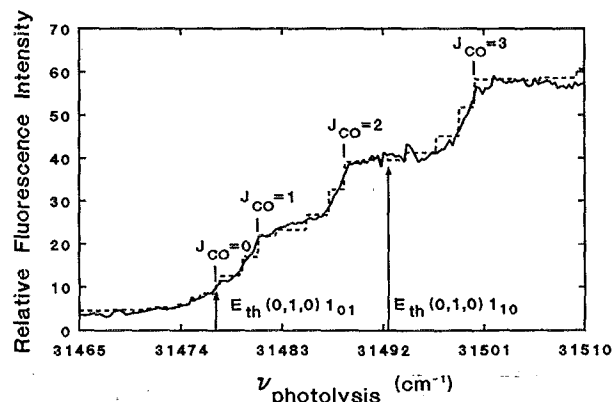


FIG. 3. The threshold region of the PHOFEX spectrum of the  $(0,1,0)1_{01}$  state with the fit described in the text, Eq. (1). The thresholds of the different CO channels are labeled as is the threshold of the next ortho state,  $1_{10}$ , of  $^1\text{CH}_2$ .

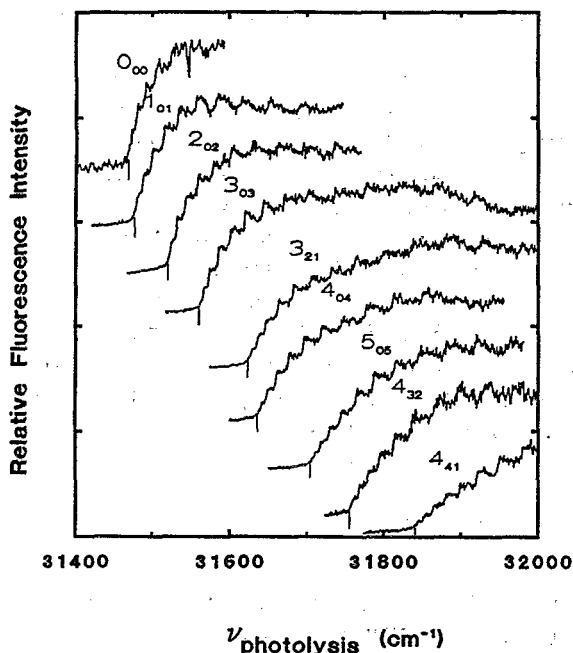


FIG. 4. PHOFEX spectra of the (0,1,0) states with the energetic thresholds, taking nuclear spin conservation into account, marked. The spectra are obtained by scanning the photolysis frequency with the probe laser fixed on the following  $\bar{b}-\bar{a}(0,1,0)$  transitions: (1)  $(0,15,0)1_{10} \leftarrow 0_{00}$  ( $16\,390.19\text{ cm}^{-1}$ ); (2)  $(0,15,0)2_{11} \leftarrow 1_{01}$  ( $16\,405.29\text{ cm}^{-1}$ ); (3)  $(0,15,0)3_{12} \leftarrow 2_{02}$  ( $16\,421.47\text{ cm}^{-1}$ ); (4)  $(0,15,0)4_{13} \leftarrow 3_{03}$  ( $16\,441.87\text{ cm}^{-1}$ ); (5)  $(0,15,0)2_{11} \leftarrow 3_{21}$  ( $16\,258.38\text{ cm}^{-1}$ ); (6)  $(0,15,0)5_{14} \leftarrow 4_{04}$  ( $16\,452.01\text{ cm}^{-1}$ ); (7)  $(0,15,0)6_{15} \leftarrow 5_{05}$  ( $16\,479.36\text{ cm}^{-1}$ ); (8)  $(0,16,0)4_{40} \leftarrow 4_{32}$  ( $16\,503.56\text{ cm}^{-1}$ ); (9)  $(0,15,0)4_{13} \leftarrow 4_{41}$  ( $16\,164.55\text{ cm}^{-1}$ ).

producing the rotational states probed and the fact that the intensity increment at each step is roughly in accord with a PST model, suggest that the *rotational* distribution of the (0,1,0) molecules is given by PST over the energy scale

TABLE I. Thresholds for the production of  $\text{CH}_2(\bar{a}^1A_1)$  from  $\text{CH}_2\text{CO}$  ( $\text{cm}^{-1}$ ).

$(v_1, v_2, v_3)$	$J_{K_a, K_c}$	$E_{\text{th}}^a$	$E_{\text{rot}}^b + D_o^c$	$E_{\text{th}} - (E_{\text{rot}} + D_o)$
para (0,1,0)	0 <sub>00</sub>	31 468.9	31 468.7	0.2
	2 <sub>02</sub>	31 522.0	31 522.3	-0.3
	4 <sub>04</sub>	31 637.3	31 637.6	-0.3
ortho (0,1,0)	1 <sub>01</sub>	31 477.0	31 486.9	-9.9 <sup>d</sup>
	3 <sub>03</sub>	31 563.4	31 573.1	-9.7
	3 <sub>21</sub>	31 624.1	31 633.8	-9.5
	5 <sub>05</sub>	31 706.4	31 715.7	-9.3
	4 <sub>32</sub>	31 757.2	31 766.7	-9.5
	4 <sub>41</sub>	31 840.7	31 850.4	-9.7
(0,2,0)	1 <sub>01</sub>	32 791.7	32 801.6	-9.9
(1,0,0)	1 <sub>01</sub>	32 930.7	32 940.2	-9.5

<sup>a</sup>Threshold energies extracted from PHOFEX curves, errors are estimated to be  $\pm 0.5\text{ cm}^{-1}$ .

<sup>b</sup> $\text{CH}_2$  term values from Refs. 25–27.

<sup>c</sup>The threshold for the singlet dissociation  $D_o = E_{\text{th}}(0_{00}) = 30\,116.2\text{ cm}^{-1}$ , Ref. 15.

<sup>d</sup>The lowest ortho state of  $\text{CH}_2\text{CO}$  is  $1_{11}$ ;  $E(1_{11}) = 9.7\text{ cm}^{-1}$ .

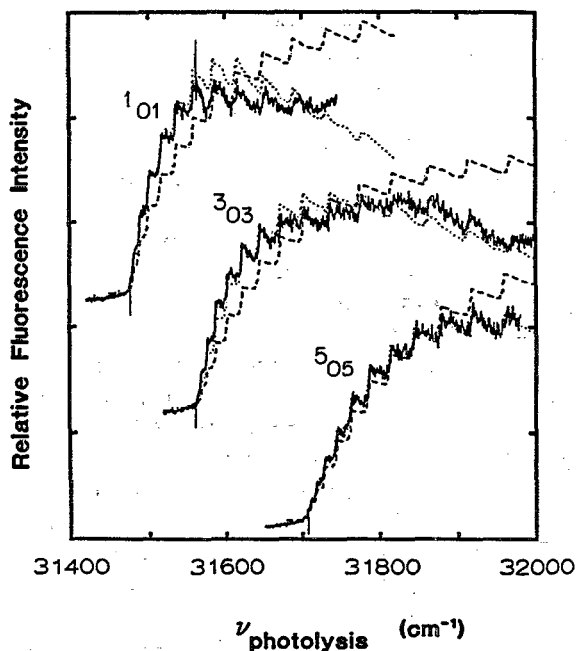


FIG. 5. PHOFEX spectra of (a)  $(0,1,0)1_{01}$  fit to PST (dashed line) and constant  $W=100$  (dotted line), (b)  $(0,1,0)3_{03}$  fit to PST (dashed line) and constant  $W=200$  (dotted line), and (c)  $(0,1,0)5_{05}$  fit to PST (dashed line), and constant  $W=300$  (dotted line).

shown here. (Naturally, it would be better to measure the rotational distribution directly with an LIF spectrum, but the unknown rotational line strengths for the highly perturbed methylene spectrum makes this difficult.) In the previous PHOFEX study,  $K_a = 0$  and 1 states were probed; the present work is extended to  $K_a$  values as large as 4. No qualitative differences are observed probing states with different  $K_a$ . The PHOFEX data do not match PST well over a long scan, Fig. 5.

A critical qualitative feature of the PHOFEX curve in Fig. 3 is the observation of steps below  $31\,492\text{ cm}^{-1}$ , where the next *ortho* methylene state  $1_{10}$  has its appearance threshold. Below this energy  $1_{01}$  is the only *ortho* (0,1,0) methylene state which is energetically accessible, and this

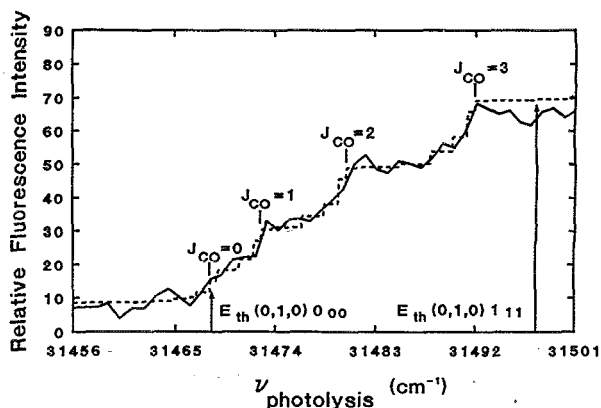


FIG. 6. The threshold region of the PHOFEX spectrum of the  $(0,1,0)0_{00}$  state fit to PST. The thresholds of the different CO channels are labeled as is the threshold of the next *para* state,  $1_{11}$ .

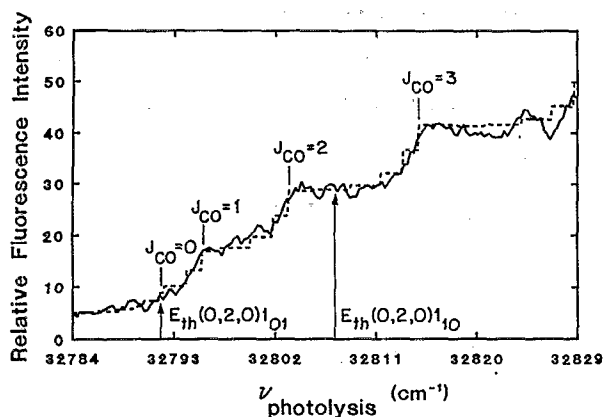


FIG. 7. The threshold region of the PHOFEX spectrum of the  $(0,2,0)_{101}$  state with the fit described in the text, Eq. (1). The thresholds of the different CO channels are labeled as is the threshold of the next *ortho* state.

PHOFEX curve is essentially the quantum yield curve for *ortho*  $(0,1,0)$ . The steps in this curve, spaced as they are by the CO free-rotor eigenvalues, clearly demonstrate that the quantum yield of  $(0,1,0)$  is determined by a "loose" transition state at large enough values of the reaction coordinate so that CO rotation is not significantly hindered. The same conclusion is reached by probing the  $(0,1,0)_{000}$  state, Fig. 6, which below  $31\,497\text{ cm}^{-1}$  is essentially the *para*  $(0,1,0)$  curve. The same qualitative features are also observed in the PHOFEX curves measured probing the  $(0,2,0)_{101}$  and the  $(1,0,0)_{101}$  states, Figs. 7 and 8, about  $3000\text{ cm}^{-1}$  above the singlet channel threshold. The important implications of the observations of loose transition states at energies where "tight" transition states must be inferred from rate measurements are discussed in Sec. V.

## B. Models

Several models have been tested against the PHOFEX curves measured in the present work. The fine structure in the PHOFEX spectra indicates that the rotational and vibrational state distributions are sensitive to the number of product states, as predicted by PST. However, PST seriously un-

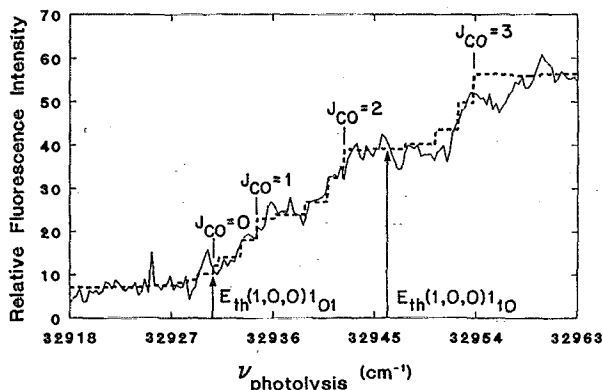


FIG. 8. The threshold region of the PHOFEX spectrum of the  $(1,0,0)_{101}$  state with the fit described in the text, Eq. (1). The thresholds of the different CO channels are labeled as is the threshold of the next *ortho* state.

derestimates the quantum yield for vibrational excitation (Sec. IV); this is exhibited indirectly in the PST fits to PHOFEX spectra, where the maxima are displaced to much higher energy than is observed experimentally, Fig. 5. The absolute intensities of the PHOFEX curves are generally unknown, so the fits presented here are normalized to match the data; if the absolute intensity of the  $(0,1,0)_{101}$  PHOFEX curve is taken from the branching ratio measurement (Sec. IV), it would be  $3\times$  as tall as the corresponding PST curve.

It is convenient to use the conditional probabilities<sup>18</sup>  $P(s)$ , the singlet quantum yield,  $P(v|s)$ , the fraction of the singlet formed in state  $v$ , and  $P(J_{K_a,K_c}|s,v)$  the fraction of product in vibrational state  $v$  which is formed in rotational state  $J_{K_a,K_c}$ , since these different degrees of freedom are usually treated separately.

In all the fits presented here, the PHOFEX signal is taken to be proportional to the product of conditional probabilities

$$\Phi(v, J_{K_a, K_c}) = P(s)P(v|s)P(J_{K_a, K_c}|s, v),$$

where the rotational state distribution  $P(J_{K_a, K_c}|s, v)$  is given by PST. From the accompanying study  $P(s)$  is known to be fairly constant in the energy range of a PHOFEX scan.<sup>14</sup> The task is then to derive the functional form of  $P(v|s)$ . One reasonable hypothesis is that near the  $(0,1,0)$  threshold the number of channels leading to  $(0,1,0)$  rises as predicted by PST, while the number of competing channels leading to  $(0,0,0)$  are only slowly varying with energy and can be fit with a constant. This model is formally identical to that used successfully to fit the  $(0,0,0)$  PHOFEX spectra previously<sup>15</sup>

$$\Phi[(0,1,0)J_{K_a, K_c}] = \frac{N_{\text{PST}}[(0,1,0)]}{(2J' + 1)W + N_{\text{PST}}[(0,1,0)]} \times \frac{N_{\text{PST}}[(0,1,0)J_{K_a, K_c}]}{N_{\text{PST}}[(0,1,0)]} \quad (1)$$

$J'$  is the ketene excited state quantum number.

With the correct choice of the constant  $W$  for the effective number of open channels to products other than  $\text{CH}_2(0,1,0)$ , this model fits the PHOFEX data very well, Fig. 5; however,  $W$  values as small as the ones needed to fit the shapes of the PHOFEX curves imply a vibrational quantum yield,  $P(v=1|s)$  5–15 times larger than the experimental value at  $31\,616.2\text{ cm}^{-1}$  (Sec. IV).

The direct rate measurements<sup>9</sup> combined with the singlet/triplet branching ratio measurements<sup>14</sup> experimentally determine the rate of increase of the total number of dissociation channels with energy. If the PST value for the rate of formation of  $(0,1,0)$  is used,

$$P(v|s) = \frac{N_{\text{PST}}[(0,1,0)]}{h\rho k_{\text{total}} P(s)} \quad (2)$$

and, assuming that the change of the denominator with energy is relatively small, the PHOFEX fitting equation

$$\Phi[(0,1,0)J_{K_a, K_c}] \approx \frac{N_{\text{PST}}[(0,1,0)J_{K_a, K_c}]}{(2J' + 1)[1 + \alpha(E - E_0)]} \quad (3)$$

or equivalently  $[1 + \alpha(E - E_0)]$  can be replaced with  $\exp[\alpha(E - E_0)]$ . Here  $\alpha$  is determined by the rate of increase

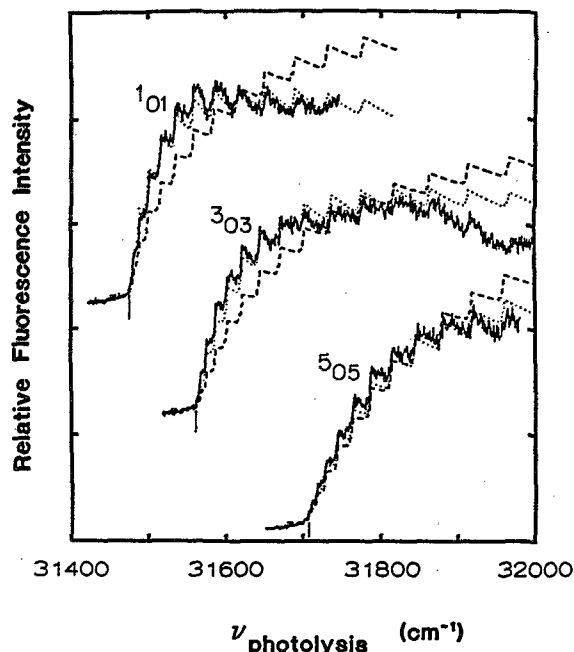


FIG. 9. PHOFEX spectra of  $(0,1,0)1_{01}$ ,  $(0,1,0)3_{03}$ , and  $(0,1,0)5_{05}$  fit to Eq. (2) with  $\alpha = 0.001$  (dashed line) and  $\alpha = 0.00525$  (dotted line).

of the dissociation rate and the density of states; using the measured dissociation rate and the Whitten–Rabinovitch expression for  $\rho$ , one obtains  $\alpha \approx 0.001 \pm 0.0005/\text{cm}^{-1}$  in the energy range of interest. This value of  $\alpha$  fits the PHOFEX data rather poorly; however, the value  $\alpha = 0.00525/\text{cm}^{-1}$  fits the PHOFEX curves for all of the  $(0,1,0)$  rotational states quite well, Fig. 9. This much larger value of  $\alpha$  cannot be due to uncertainties in the rate measurements. It seems very unlikely that the Whitten–Rabinovitch estimate<sup>1</sup> of the relative rate of increase of the density of states is so much in error. Instead it appears that the fit parameter  $\alpha$  is compensating primarily for the overestimate by PST of the increase in the effective number of  $(0,1,0)$  dissociation channels with energy; this effect is predicted by the variational RRKM calculations of Klippenstein and Marcus. Their calculated PHOFEX curves are published separately.<sup>20</sup>

The separate statistical ensembles (SSE) method predicts rovibrational distributions, and so can easily be compared with the PHOFEX data. In SSE, the vibrational quantum yield  $P(v|s)$  is proportional to the density of states of an unhindered ensemble of dimension equal to the number of disappearing oscillators given the total excess energy. The SSE prediction is simply

$$P(v|s) = (E - h\nu_2)^{1.5} / \{(E - h\nu_2)^{1.5} + E^{1.5}\}, \quad (4)$$

where  $E$  is the available energy above the singlet channel threshold. This prediction matches the experimental PHOFEX curves quite well everywhere except close to the threshold of the vibrational channel (Fig. 10), where the formula for  $P(v|s)$  is smooth, but the experimental data indicates that it should be highly structured. However, it is quite remarkable that such a simple model without adjustable parameters, does so well.

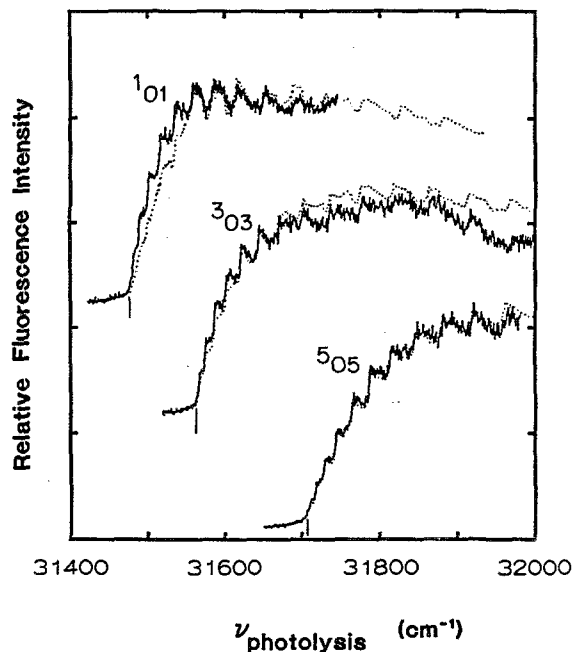


FIG. 10. PHOFEX spectra of  $(0,1,0)1_{01}$ ,  $(0,1,0)3_{03}$ , and  $(0,1,0)5_{05}$  fit to the SSE model. Note the discrepancy near the threshold of the  $(0,1,0)1_{01}$  curve.

## IV. THE $(0,1,0)$ QUANTUM YIELD

### A. Results

The primary experimental datum is the ratio of the fluorescence signal observed photolyzing ketene at  $\nu_1 = 31564.8 \text{ cm}^{-1}$  and probing the methylene  $\bar{b}(0,15,0)2_{11} \leftarrow \bar{a}(0,1,0)1_{01}$  transition through the blue filter stack to that observed photolyzing at  $\nu_0 = 30299.4 \text{ cm}^{-1}$  and probing  $\bar{b}(0,15,0)2_{11} \leftarrow \bar{a}(0,0,0)1_{01}$  through the red filters. Both signals are normalized to the incident uv power; the measured ratio is  $0.199 \pm 0.011$ . The uncertainty quoted is the standard deviation of several experimental measurements. Several factors are needed to convert the experimental relative intensity measurements into  $(0,1,0)$  quantum yield measurements suitable for comparison with Klippenstein and Marcus's theoretical predictions.<sup>19</sup> To account for the different filters, the experimental ratio must be divided by the measured blue:red sensitivity ratio of  $2.8 \pm 0.3$ . Because the quantum yield is defined relative to the number of uv photons rather than to the uv power, the ratio must be multiplied by  $\nu_0/\nu_1$ . The ratio must also be multiplied by the ratio of absorption cross section of ketene at  $\nu_0$  to that at  $\nu_1$ . From the room-temperature absorption spectrum, a factor of  $1.02 \pm 0.02$  is derived. Multiplying by all these factors yields a ratio of the quantum yield  $\Phi[(0,1,0)1_{01}]$  at  $\nu_1$  to  $\Phi[(0,0,0)1_{01}]$  at  $\nu_0$  of  $0.075 \pm 0.008$ . The  $(0,1,0)1_{01}$  PHOFEX curve measured in this work, appropriately corrected for the ketene absorption cross section, provides a direct experimental measurement of the change in  $\Phi[(0,1,0)1_{01}]$  with energy. Making the conversion to  $31616.2 \text{ cm}^{-1}$ , the energy where Klippenstein and Marcus calculated the vibrational branching ratio theoretically, the experimental ratio becomes  $0.073 \pm 0.008$ .

## B. Variational RRKM

Klippenstein and Marcus<sup>19</sup> have calculated the vibrational excitation probability of the singlet channel  $P(v|s)$  at  $31\,616.2\text{ cm}^{-1}$  ( $1500\text{ cm}^{-1}$  above the singlet channel threshold) using a variational RRKM technique. Marcus<sup>18</sup> originally proposed two different methods for calculating the vibrational excitation probability. Klippenstein and Marcus<sup>19,20</sup> implemented the method in which the vibrational excitation probability is sensitive to different transition states on vibrationally adiabatic curves for (0,0,0) and (0,1,0). This method is consistent with the observation here of loose transition states for vibrational channels near their threshold, Figs. 3 and 6–8. Klippenstein and Marcus actually calculated two values for the branching ratio due to the occurrence of multiple minima in the number of (0,1,0) states at sufficiently high energies. Considering only one of the minima yields  $P(v_2 = 1|s) = 0.030$ . Considering the multiple minima explicitly yields a value of 0.025. Marcus' theory also predicts the rotational state distributions  $P(J_{K_a, K_c} | s, v)$  for each vibrational state, which are essentially given by PST.<sup>18,19</sup> The "rotational quantum yield"  $P(1_{01} | s, v_2 = 1)$  for the  $1_{01}$  state of (0,1,0) at  $31\,616.2\text{ cm}^{-1}$  is calculated by PST to be 0.193; similarly,  $P(1_{01} | s, v = 0)$  is calculated to be 0.132 at  $\nu_0$ .  $P(v = 0|s) = 1$  at  $\nu_0$ , since no other singlet vibrational channels are energetically accessible at that photolysis wavelength. The values of  $P(s)$  are derived from Fig. 5 of Ref. 14 as  $0.43 \pm 0.03$  and  $0.72 \pm 0.06$  at  $\nu_0$  and  $\nu_1$ , respectively. The experimental ratio of  $0.073 \pm 0.008$  derived above can then be compared with Klippenstein and Marcus' theoretical ratios of  $[P(s; \nu_1)P(v_2 = 1|s; \nu_1)P(1_{01} | s, v_2 = 1; \nu_1)] / [P(s; \nu_0)P(v = 0|s; \nu_0)P(1_{01} | s, v = 0; \nu_0)] = 0.073 \pm 0.008$  and  $0.061 \pm 0.007$  from the two different ways of treating the multiple minima. By contrast, PST predicts a ratio of  $0.023 \pm 0.002$ , a factor of about 2 to 3 smaller than Klippenstein and Marcus' prediction, while SSE predicts  $0.073 \pm 0.008$ . The error bars given here on the theoretical values reflect only the uncertainty in the singlet/triplet branching ratio. Inverting this procedure allows estimation of an experimental  $P(v_2 = 1|s)$ , Table II. The agreement between experiment and Klippenstein and Marcus' prediction is surprisingly good, especially since the parameters of their model potential energy surface were chosen before the experiments were completed. The data also include some thermal averaging effects, while their calculation was restricted to  $J'(\text{CH}_2\text{CO}) = 3$ .

Combining the experimental rate, singlet/triplet branching ratio, and vibrational quantum yield measure-

ments allows an experimental estimate of the dissociation rate on the singlet surface to form (0,1,0) methylene at a photolysis energy of  $31\,616.2\text{ cm}^{-1}$ :  $(9 \pm 2) \times 10^7\text{ s}^{-1}$ . This value will be affected by the uncertain effects of rotational averaging on the different experimental measurements. This rate is a factor of 3 smaller than that predicted by PST using the Whitten–Rabinovitch density of states.

## V. DISCUSSION AND CONCLUSIONS

The PHOFEX spectra of vibrationally excited singlet methylene produced by the variable wavelength photolysis of jet-cooled ketene have been measured, as well as the vibrational branching ratio at one photolysis wavelength. The energetic thresholds, the fine structure in the PHOFEX spectra, the branching ratio measurements and the absolute rate data<sup>9</sup> each have important implications; together they provide a discriminating test of theories of unimolecular dissociation on barrierless potential energy surfaces.

The experiments demonstrate conclusively that there are no barriers to the dissociation—all of the experimental thresholds match the values expected from the methylene and CO term values, taking into account the conservation of nuclear spin and the small thermal energy of jet-cooled ketene. This is true even for the state (0,1,0) $4_{41}$ , which has  $382\text{ cm}^{-1}$  of rotational energy. Under conditions for which the statistical adiabatic channel model (SACM)<sup>5–7</sup> predicts rates less than the PST rate, it predicts dynamical barriers which increase in size with product rotational energy—no barriers to formation of final product states are detected with an energy resolution of  $0.5\text{ cm}^{-1}$ . Despite its success at fitting other types of data from many systems, SACM does not predict the product thresholds and energy state distributions observed near threshold for ketene. No model which postulates dynamical barriers that raise product thresholds is consistent with the results here. If it is assumed that the channels are adiabatic only through the region of channel maxima and that rotations are completely mixed as fragments subsequently separate, SACM predicts rate constants and rotational distributions qualitatively similar to those of variational RRKM. However, this uncoupling and subsequent recoupling of degrees of freedom as the fragments separate seems unphysical to us.

The observation of steps spaced by the CO rotational energies in the singlet methylene (0,1,0), (0,2,0), and (1,0,0)  $J_{K_a, K_c}$  PHOFEX curves similar to those observed previously for (0,0,0)<sup>15,16</sup> suggests that the rotational state distribution within a specific vibrational state is given by PST. This is assumed in both SSE and the new variational RRKM

TABLE II. Vibrational excitation probability  $P(v_2 = 1|s)$   $1500\text{ cm}^{-1}$  above the singlet threshold.

Experiment <sup>a</sup>	PST	Variational RRKM	SSE	Fitting model <sup>b</sup>
$0.030 \pm 0.005$	0.0094	0.025 <sup>c</sup> , 0.030 <sup>d</sup>	0.030	0.16–0.37

<sup>a</sup> Derived from the experimental data assuming PST rotational state distributions. See Sec. IV B.

<sup>b</sup> Using  $300 > W > 100$  in Eq. (1).

<sup>c</sup> Calculated considering all minima in the number of states, Ref. 19.

<sup>d</sup> Calculated considering only one minimum in the number of states, Ref. 19.

theory. However, a direct measurement of the methylene rotational state distribution is needed to check this, especially well above threshold, where the large energy level spacings in  $^1\text{CH}_2$  could inhibit energy flow. The singlet channel CO fragment rotational state distribution is in accord with PST predictions up to  $2500\text{ cm}^{-1}$  above threshold, though at the top of this energy range overlapping contributions from the triplet channel make this measurement less discriminating.<sup>14</sup> So far all experimental results indicate that energy flows freely among the degrees of freedom corresponding to product rotation and translation until the products are effectively separated.

The presence of steps in the (0,1,0)  $0_{00}$  and  $1_{01}$  PHOFEX curves below the threshold for production of any other methylene states of the same vibrational and nuclear spin state is particularly important. Only one methylene rotational state is energetically accessible,  $P(J_{K_a K_c} | v_2 = 1, s) = 1$ , so the steps must be due to  $P(v|s)$ . The vibrational branching ratio increases as each new CO( $J$ ) channel opens at its free-rotor term value. This can only occur if the vibrational branching ratio is determined by the properties of a loose transition state whose energy levels are very nearly those of the isolated fragments. The observation of similar behavior for the (0,2,0) and (1,0,0) vibrational states suggests that near-threshold vibrational quantum yields may generally be determined by loose transition states. This result clearly rules out the hypothesis that the vibrational state distribution is determined early in the dissociation, at a small value of the reaction coordinate where the energy level spacings would be much larger than those of a free rotor, a major premise of Rosenfeld's early phase space theory<sup>31</sup> and one of the alternative hypotheses suggested by Marcus.<sup>18</sup> The predictions of the separate statistical ensembles (SSE) theory<sup>10</sup> are generally in agreement with our results; however, the present form of SSE does not predict the quantized fine structure very near the vibrational channel thresholds. The success of the very simple SSE model suggests that refinement of this theory to include quantum effects would be worthwhile. Since the underlying physical assumptions of SSE and variational RRKM are significantly different, it will be important to test them in regimes where significantly different results are predicted.

The observed near-threshold steps in the PHOFEX spectra are part of the newest version of variational RRKM theory<sup>18,19</sup> which considers each vibrationally adiabatic curve to have its own transition state, Fig. 11. Near a vibrational threshold, that channel's transition state (c) will lie far out on the adiabatic curve leading to vibrationally excited products, and many dissociation trajectories reflect at this bottleneck, eventually finding their way back past (a) and onto other adiabatic curves. This competition between channels, restricted by a very loose transition state, makes  $P(v|s)$  sensitive to energy spacings nearly equal to the free-rotor spacings of the fragments, which are manifested in the PHOFEX spectra. Thus the vibrational branching ratios are not given by the branching between vibrationally adiabatic surfaces which occurs at point a in Fig. 11 as the molecule moves out along the reaction coordinate, but rather by the number of channels at the vibrational TS on each surface.

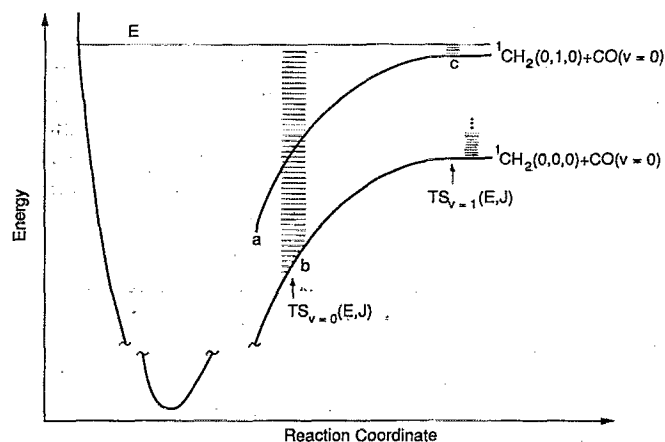


FIG. 11. Schematic diagram of a variational RRKM model consistent with the present data. An adiabatic potential and a corresponding transition state surface are defined for each product vibrational state. As total energy increases above the asymptotic threshold for each channel the transition state moves in along the reaction coordinate. The increase in level spacing as the chemical bond tightens decreases the number of states  $W_v(E, J)$  and hence the rate constant with respect to the phase space theory limit (transition state at fully separated products). The relative population of an excited vibrational state,  $N_{v=1}(c)/N_{v=0}(b)$ , is larger than in PST where both transition states are at the product end of the reaction coordinate. In the calculations of Klippenstein and Marcus (Refs. 18 and 19) point a where the vibration becomes adiabatic is taken to be identical to point b, the transition state on the ground state surface. In general, point a will be different for each vibrational coordinate and not closely related to point b which must move as total energy changes.

The (0,1,0) quantum yield measurement, consistent with the experimental results from NCNO<sup>10</sup> and various theoretical predictions, indicates that PST underestimates the excitation of product vibrations. While the near-threshold steps in the PHOFEX spectra show that the (0,1,0) quantum yield is determined at a loose transition state, the quantum yield measurement indicates that the effective number of (0,0,0) channels is restricted. The fits to the PHOFEX curves and the recent rate measurements in the Zewail group<sup>9</sup> provide further evidence that (0,0,0) has a tight transition state at energies above the threshold for product vibrational excitation.

The results reported to date on ketene are qualitatively consistent with a variational form of RRKM theory. Quantitative predictions, often in advance of the experimental results have been remarkably accurate even though potential surface shapes had to be guessed. A number of models are clearly excluded by the data. It is possible that interesting new models will also be consistent with the results obtained so far. It will be important to understand at what point each vibrational degree of freedom becomes adiabatic as the chemical bond breaks. For most vibrations one imagines that point a, Fig. 11, for each vibration will lie at or inside of b as shown. However, for soft product degrees of freedom such as internal rotation or torsion a may well lie outside of b. Further experimental data and accurate *ab initio* potential energy surfaces will be required to test models which treat vibrational adiabaticity in detail for unimolecular reactions without barriers.

## ACKNOWLEDGMENTS

We are grateful to S. J. Klippenstein, R. A. Marcus, and A. H. Zewail for providing their results to us prior to publication. We are particularly grateful to R. A. Marcus, whose active interest in these results led to the swift development of a new theoretical model, and to S. J. Klippenstein, whose collaboration in comparing theory with our experimental results proved very stimulating. We would also like to thank C. D. Pibel, who developed the software used in recording the PHOFEX spectra and C. Wittig for valuable comments on the manuscript. This work was supported by the National Science Foundation, under Grant No. CHE88-16552. W.H.G. thanks the Amoco Foundation for fellowship support. Q.K.Z. is grateful to the U.C. Berkeley-Fudan University Exchange Program, which made her visit to the U.S. possible.

<sup>1</sup> P. J. Robinson and K. A. Holbrook, *Unimolecular Reactions* (Wiley, London, 1972).

<sup>2</sup> W. Forst, *Theory of Unimolecular Reactions* (Academic, New York, 1973).

<sup>3</sup> P. Pechukas and J. C. Light, *J. Chem. Phys.* **42**, 3281 (1965).

<sup>4</sup> C. E. Klots, *J. Phys. Chem.* **75**, 1526 (1971).

<sup>5</sup> M. Quack and J. Troe, *Ber. Bunsenges. Phys. Chem.* **78**, 240 (1974).

<sup>6</sup> M. Quack and J. Troe, *Ber. Bunsenges. Phys. Chem.* **79**, 170 (1975).

<sup>7</sup> M. Quack and J. Troe, *Ber. Bunsenges. Phys. Chem.* **79**, 469 (1975).

<sup>8</sup> L. R. Khundar and A. H. Zewail, *J. Chem. Phys.* **87**, 77 (1987).

<sup>9</sup> E. D. Potter, M. Gruebele, L. R. Khundkar, and A. H. Zewail, *Chem. Phys. Lett.* **164**, 463 (1989).

<sup>10</sup> C. Wittig, I. Nadler, H. Reisler, J. Catanzarite, and G. Radhakrishnan, *J. Chem. Phys.* **83**, 5581 (1985).

<sup>11</sup> D. J. Nesbitt, H. Petek, M. F. Foltz, S. V. Filseth, D. J. Bamford and C. B. Moore, *J. Chem. Phys.* **83**, 223 (1985).

<sup>12</sup> T. M. Ticich, T. R. Rizzo, H. R. Dübal, and F. F. Crim, *J. Chem. Phys.* **84**, 1508 (1986).

<sup>13</sup> A. Sinha, R. L. Vander Wal, and F. F. Crim, *J. Chem. Phys.* **92**, 401 (1990).

<sup>14</sup> S. K. Kim, Y. S. Choi, C. D. Pibel, Q.-K. Zheng and C. B. Moore *J. Chem. Phys.* **94**, 1954 (1991).

<sup>15</sup> I.-C. Chen, W. H. Green, and C. B. Moore, *J. Chem. Phys.* **89**, 314 (1988).

<sup>16</sup> W. H. Green, I.-C. Chen, and C. B. Moore, *Ber. Bunsenges. Phys. Chem.* **92**, 389 (1988).

<sup>17</sup> W. H. Green, Jr., Ph.D. dissertation, University of California, Berkeley, 1988.

<sup>18</sup> R. A. Marcus, *Chem. Phys. Lett.* **144**, 208 (1988).

<sup>19</sup> S. J. Klippenstein and R. A. Marcus, *J. Chem. Phys.* **91**, 2280 (1989).

<sup>20</sup> S. J. Klippenstein and R. A. Marcus, *J. Chem. Phys.* **93**, 2418 (1989).

<sup>21</sup> J. Troe, *J. Chem. Phys.* **85**, 1708 (1986); C. Wittig, I. Nadler, H. Reisler, J. Catanzarite, and G. Radhakrishnan, *ibid.* **85**, 1710 (1986).

<sup>22</sup> H. Reisler and C. Wittig, *Annu. Rev. Phys. Chem.* **37**, 307 (1986).

<sup>23</sup> W. D. Allen and H. F. Schaefer, *J. Chem. Phys.* **89**, 329 (1988); **84**, 2212 (1986).

<sup>24</sup> P. R. Bunker, P. Jensen, W. P. Kraemer, and R. Beardsworth, *J. Chem. Phys.* **85**, 3724 (1986).

<sup>25</sup> H. Petek, D. J. Nesbitt, D. C. Darwin, and C. B. Moore, *J. Chem. Phys.* **86**, 1172 (1987).

<sup>26</sup> H. Petek, D. J. Nesbitt, D. C. Darwin, P. R. Ogilby, C. B. Moore, and D. A. Ramsay, *J. Chem. Phys.* **91**, 6566 (1989).

<sup>27</sup> W. Xie, C. Harkin, H.-L. Dai, W. H. Green, Q.-K. Zheng, and A. J. Mahoney, *J. Mol. Spectrosc.* **138**, 596 (1989).

<sup>28</sup> I.-C. Chen and C. B. Moore, *J. Phys. Chem.* **94**, 263 and 269 (1990).

<sup>29</sup> W. H. Green, I.-C. Chen, H. Bitto, D. R. Guyer, and C. B. Moore, *J. Mol. Spectrosc.* **138**, 614 (1989).

<sup>30</sup> J. W. Rabalais, J. M. McDonald, V. Scherr, and S. P. McGlynn, *Chem. Rev.* **71**, 73 (1971).

<sup>31</sup> J. P. Holland and R. N. Rosenfeld, *J. Chem. Phys.* **89**, 7217 (1988).